JACS
JOURNAL OF THE AMERICAN CHEMICAL SOCIETY

ARTICLE

pubs.acs.org/JACS

Macrocyclic β-Sheet Peptides That Inhibit the Aggregation of a Tau-Protein-Derived Hexapeptide

Jing Zheng,[†] Cong Liu,[‡] Michael R. Sawaya,[‡] Balraju Vadla,[†] Shafiullah Khan,[†] R. Jeremy Woods,[†] David Eisenberg,[‡] Warren J. Goux,[§] and James S. Nowick*[,†]

[†]Department of Chemistry, University of California, Irvine, Irvine, California 92697-2025, United States

[‡]Howard Hughes Medical Institute, UCLA-DOE Institute of Genomics and Proteomics, Los Angeles, California 90095-1570, United States

[§]Department of Chemistry, University of Texas at Dallas, Richardson, Texas 75080, United States

Supporting Information

ABSTRACT: This paper describes studies of a series of macrocyclic β-sheet peptides **1** that inhibit the aggregation of a tau-protein-derived peptide. The macrocyclic β-sheet peptides comprise a pentapeptide "upper" strand, two δ-linked ornithine turn units, and a "lower" strand comprising two additional residues and the β-sheet peptidomimetic template "Hao". The tau-derived peptide Ac-VQIVYK-NH_2 (AcPHF6) aggregates in solution through β-sheet interactions to form straight and twisted filaments similar to those formed by tau protein in Alzheimer's neurofibrillary tangles. Macrocycles **1** containing the pentapeptide VQIVY in the "upper" strand delay and suppress the onset of aggregation of the AcPHF6 peptide. Inhibition is particularly pronounced in macrocycles **1a**, **1d**, and **1f**, in which the two residues in the "lower" strand provide a pattern of hydrophobicity and hydrophilicity that matches that of the pentapeptide "upper" strand. Inhibition varies strongly with the concentration of these macrocycles, suggesting that it is cooperative. Macrocycle **1b** containing the pentapeptide QIVYK shows little inhibition, suggesting the possibility of a preferred direction of growth of AcPHF6 β-sheets. On the basis of these studies, a model is proposed in which the AcPHF6 amyloid grows as a layered pair of β-sheets and in which growth is blocked by a pair of macrocycles that cap the growing paired hydrogen-bonding edges. This model provides a provocative and appealing target for future inhibitor design.

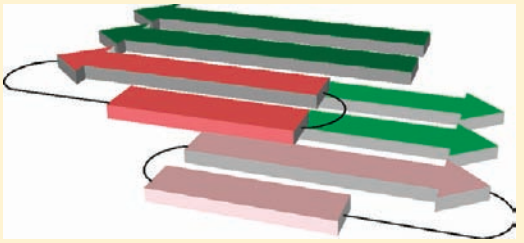

INTRODUCTION

The layered structures of parallel β-sheets are emerging as a common feature in protein and peptide aggregation associated with amyloid diseases.[1−7] Pathological amyloid fibrils contain β-sheet-rich structures in which the β-strands extend roughly perpendicular to the fibril elongation axis. Recent advances in solid-state NMR spectroscopy, X-ray crystallography, and other techniques have revealed the architecture of many of these β-sheet amyloids at atomic resolution. In many amyloidogenic proteins and peptides, the core structure of the resulting fibril contains a pair of parallel in-register β-sheets layered in an antiparallel fashion. Figure 1 illustrates this *antiparallel-layered parallel β-sheet* structure with a cartoon.

Antiparallel-layered parallel β-sheets are central to protein and peptide aggregation in amyloid-related neurodegenerative diseases, including Alzheimer's disease and prion diseases. Alzheimer's disease features extracellular amyloid plaques formed by β-amyloid peptides (Aβ) and intracellular neurofibrillary tangles (NFTs) formed by the protein tau.[8] NFTs also exist in other neurodegenerative diseases such as frontotemporal dementia with parkinsonism linked to chromosome 17. These related diseases and Alzheimer's disease are collectively termed tauopathies.[9]

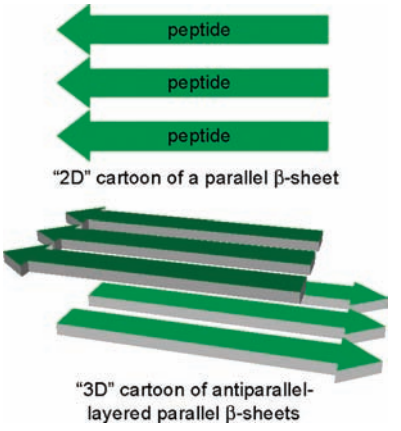

Figure 1. Illustrations of the two-dimensional structure of a parallel β-sheet and the three-dimensional structure of antiparallel-layered parallel β-sheets.

The microtubule-associated protein tau binds to and stabilizes microtubules and is crucial in regulating neurite extension. In various

Received: November 23, 2010
Published: February 14, 2011

 © 2011 American Chemical Society

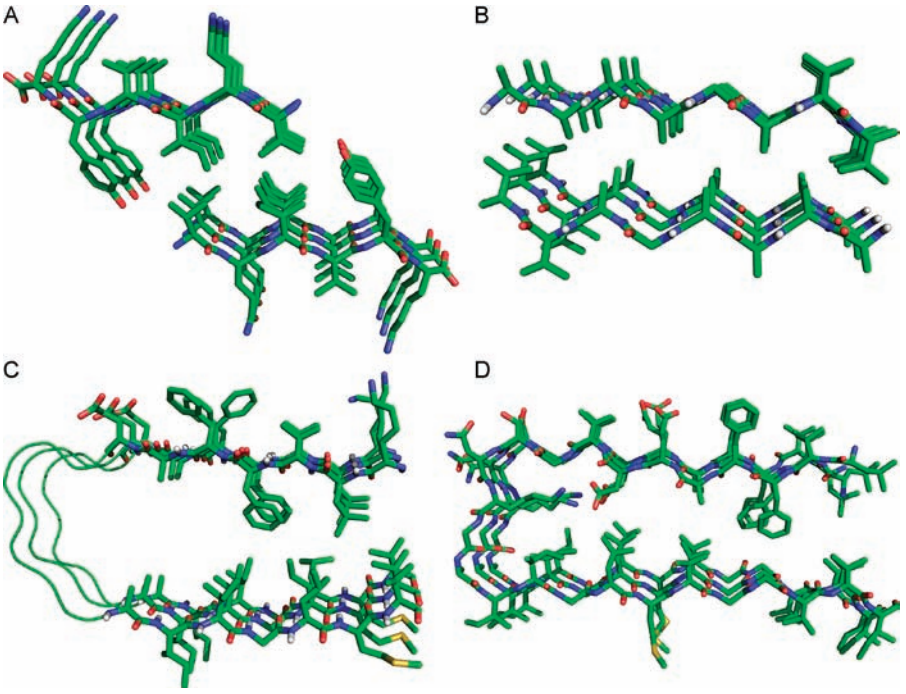

Figure 2. Antiparallel-layered parallel β-sheets associated with neurodegenerative diseases. (A) X-ray crystallographic structure of the tau-derived VQIVYK peptide.[3b] (B) NMR-based structural model of $PrP_{106-126}$ fibrils showing central residues $A_{115}-V_{122}$.[7] (C) NMR-based structural model of $A\beta_{1-40}$ fibrils showing central residues $K_{17}-D_{23}$ and $A_{31}-V_{37}$.[1b,14] (D) NMR-based structural model of $A\beta_{1-42}$ fibrils showing central residues $L_{18}-I_{42}$.[2a] All figures are depicted in projection down the fibril (or related crystal) axis and are generated by PyMOL.[15]

tauopathies, tau protein falls off microtubules to aggregate into paired helical filaments (PHFs), which further assemble into NFTs.[10] The six amino acid sequence VQIVYK ($tau_{306-311}$), located in the third repeat domain of tau, nucleates β-sheet structure and induces protein aggregation into PHFs.[11] A high-resolution X-ray crystallographic structure of the VQIVYK peptide shows antiparallel-layered parallel β-sheet structure (Figure 2A).[3b,12] Spin-labeling electron paramagnetic resonance spectroscopic studies on tau protein show that residues $tau_{303-320}$ (including VQIVYK) form a parallel in-register β-sheet structure, and these β-sheets may be layered.[13] The amyloid-like fibrils formed by a peptide fragment of the human prion protein, $PrP_{106-126}$, also feature an antiparallel-layered parallel β-sheet structure (Figure 2B).[7] In β-amyloid fibrils, the Aβ peptides fold back on themselves to form two layers of parallel β-sheets. Structural models of the two variants ($A\beta_{1-40}$ and $A\beta_{1-42}$) both comprise antiparallel-layered parallel β-sheets (Figure 2C,D).[1b,2a]

These antiparallel-layered parallel β-sheets share three common features: edge-to-edge hydrogen-bonding interaction within the parallel β-sheets, in-register orientation of like side chains among the β-strands comprising the β-sheets, and face-to-face interaction between the β-sheet layers. Thus, the X-ray crystallographic structure of the VQIVYK peptide (Figure 2A) shows parallel in-register β-sheets in which the side chains are aligned and packed together like forks, spoons, and knives in a silverware drawer. Two of these β-sheet layers are paired in a face-to-face fashion to form a sandwich-like structure in which the parallel β-sheets are aligned in an antiparallel fashion. The isoleucine and valine groups in the top and bottom β-sheet layers are packed against each other to create a hydrophobic core. The NMR-based structure of the $PrP_{106-126}$ peptide fragment (Figure 2B) shows similar features in that the alanine groups and valine groups in the two β-sheet layers interdigitate with each other to form a hydrophobic core. Both peptide fragments VQIVYK and $PrP_{106-126}$ form β-sheet layers from *identical* peptide strands. The full-length $A\beta_{1-40}$ and $A\beta_{1-42}$ peptides (Figure 2C,D) fold back on themselves to form two *different* β-sheets layers tethered by a loop region. These β-sheet layers also comprise parallel in-register β-sheets. The structure of $A\beta_{1-40}$ shows prominent face-to-face hydrophobic interactions among the phenylalanine and leucine groups in the top layer and the isoleucine, leucine, and valine groups in the bottom layer; the structure of $A\beta_{1-42}$ shows similar hydrophobic interactions among the alanine and phenylalanine groups in the top layer and the valine and glycine groups in the bottom layer.[16]

To gain insights into the interactions of antiparallel-layered parallel β-sheets, we chose to study the $tau_{306-311}$-derived peptide Ac-VQIVYK-NH_2 (AcPHF6) as a simple model for protein and peptide aggregation.[17−19]

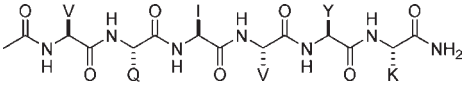

AcPHF6 peptide (based on $tau_{306-311}$)

Specifically we have used macrocyclic peptide inhibitors as molecular probes to explore molecular recognition in the aggregation and inhibition of antiparallel-layered parallel β-sheets. Goux and co-workers developed AcPHF6 as a model system of tau aggregation.[19] AcPHF6 contains the key sequence VQIVYK, which nucleates tau aggregation. AcPHF6 forms amyloid-like fibrils with the same β-sheet structure found in full-length tau amyloid fibrils, while the unadorned peptide VQIVYK does not aggregate under similar experimental conditions.[19a] Infrared spectroscopic studies suggest that AcPHF6, like the VQIVYK peptide in Figure 2A, also forms parallel β-sheets.[19a] AcPHF6 parallel β-sheets are likely in-register and layered like the

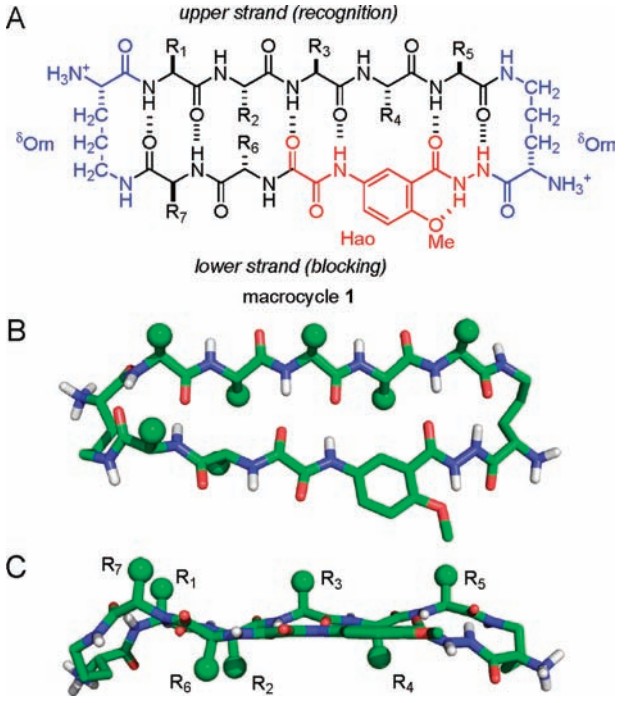

Figure 3. (A) Structure of macrocycle **1**. (B) Molecular model of macrocycle **1** (top view). (C) Molecular model of macrocycle **1** (side view) illustrating the facial positions of amino acid side chains R_1-R_7. The model is a minimum-energy conformer (local minimum) of the all-alanine analogue of macrocycle **1** ($R_1-R_7 = CH_3$) as calculated using Macromodel V6.5 with the MMFFs force field and GB/SA water solvation.

VQIVYK peptide. The atomic-level details of the VQIVYK crystal structure thus provide a structural basis to design inhibitors of AcPHF6 aggregation and to investigate the molecular recognition involved in aggregation and inhibition.

Here we describe the study of a series of macrocyclic β-sheet peptides **1** that delay and suppress the onset of AcPHF6 aggregation. Our research group (J.S.N.) previously introduced macrocycle **1** as water-soluble β-sheet structure mimics.[20] Macrocycle **1** contains a pentapeptide (R_1-R_5) in the "upper" strand, the molecular template Hao, and two additional residues (R_6 and R_7) in the "lower" strand. Hao (red in Figure 3A) is a tripeptide β-strand surrogate that templates the folding of the upper strand and blocks the hydrogen-bonding functionality of the lower strand.[21,22] The upper and lower strands of macrocycle **1** are linked by two δ-linked ornithines, which mimic β-turns (Figure 3A).[23] In the present work we incorporated AcPHF6-related pentapeptide sequences (VQIVY and QIVYK) into the upper strand of macrocycle **1**. The upper strand exposes hydrogen-bonding edges similar to those of AcPHF6 β-sheets and thus should bind to AcPHF6 by means of β-sheet interactions. The molecular template Hao in the lower strand should block further hydrogen-bonding interactions and prevent β-sheet aggregation. The two additional residues R_6 and R_7 allow tuning the folding, solubility, and side-chain hydrophobicity of the macrocycle without changing the upper strand. Figure 3B illustrates the structure of macrocycle **1** with a molecular model. Macrocycle **1** has two distinct faces, one formed by residues R_1, R_3, R_5, and R_7 and the other formed by residues R_2, R_4, and R_6 (Figure 3C). We studied the effect of macrocycle **1** on AcPHF6 aggregation by designing, synthesizing, and evaluating macrocycles that target

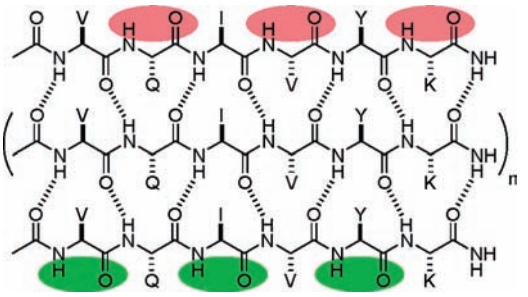

Figure 4. The two hydrogen-bonding edges of an AcPHF6 β-sheet, illustrated with red and green ovals.

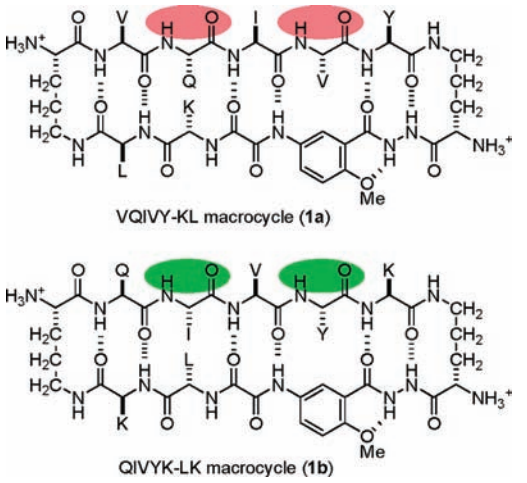

Figure 5. Macrocycles **1a** and **1b** mimic the two hydrogen-bonding edges of an AcPHF6 β-sheet. The red and green ovals illustrate hydrogen-bonding groups and match those shown in Figure 4.

the two different edges of AcPHF6 β-sheets and present different patterning of hydrophobicity and hydrophilicity of the side chains at R_6 and R_7.

RESULTS AND DISCUSSION

1. Macrocycles 1a and 1b: The Two Edges of AcPHF6 Parallel β-Sheets. We designed two macrocycles to target the two edges of AcPHF6 β-sheets. Parallel in-register β-sheets present two distinct hydrogen-bonding edges. Figure 4 illustrates this idea with a parallel in-register β-sheet formed by AcPHF6. One edge, highlighted with red ovals, presents the glutamine, valine, and lysine NH and carbonyl groups. The other edge, highlighted with green ovals, presents the valine, isoleucine, and tyrosine NH and carbonyl groups.

Pentapeptide sequence VQIVY ($tau_{306-310}$) and pentapeptide sequence QIVYK ($tau_{307-311}$) were incorporated into the respective R_1-R_5 positions in the upper strands of the VQIVY-KL macrocycle (**1a**) and the QIVYK-LK macrocycle (**1b**).[24] Macrocycle **1a** presents an upper strand that mimics the "red" hydrogen-bonding edge of AcPHF6 and thus should complement the "green" hydrogen-bonding edge of an AcPHF6 β-sheet; macrocycle **1b** presents an upper strand that mimics the "green" hydrogen-bonding edge of AcPHF6 and thus should complement the "red" hydrogen-bonding edge of an AcPHF6 β-sheet (Figure 5).

The residues at R_6 and R_7 were chosen between leucine and lysine to match the hydrophobicity and hydrophilicity of the R_1

dx.doi.org/10.1021/ja110545h | J. Am. Chem. Soc. 2011, 133, 3144–3157

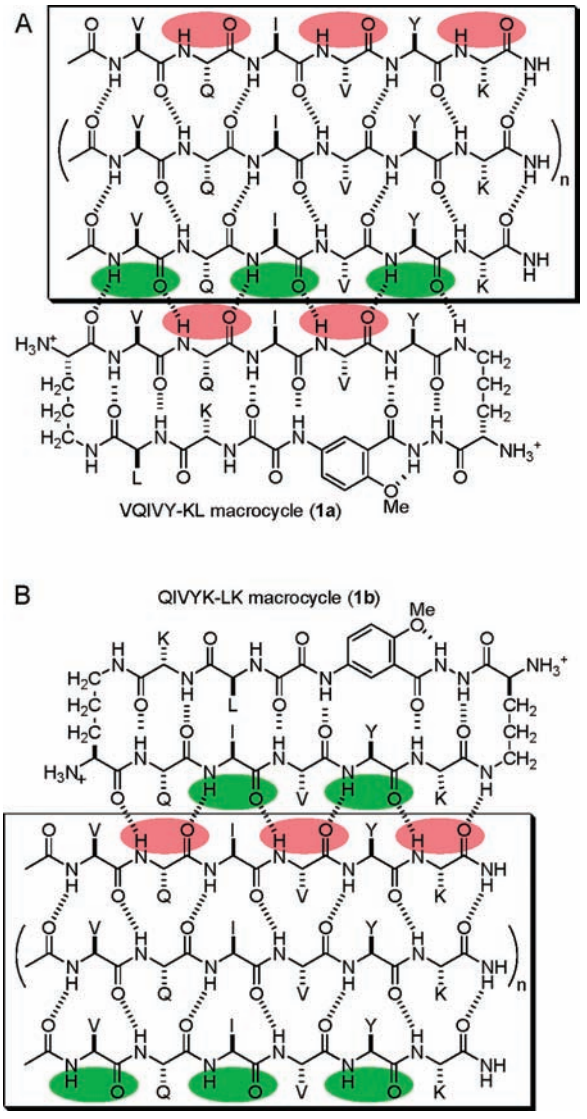

Figure 6. (A) Model of macrocycle **1a** binding to the "green" hydrogen-bonding edge of an AcPHF6 β-sheet through parallel in-register β-sheet interactions. (B) Model of macrocycle **1b** binding to the "red" hydrogen-bonding edge of an AcPHF6 β-sheet through parallel in-register β-sheet interactions.

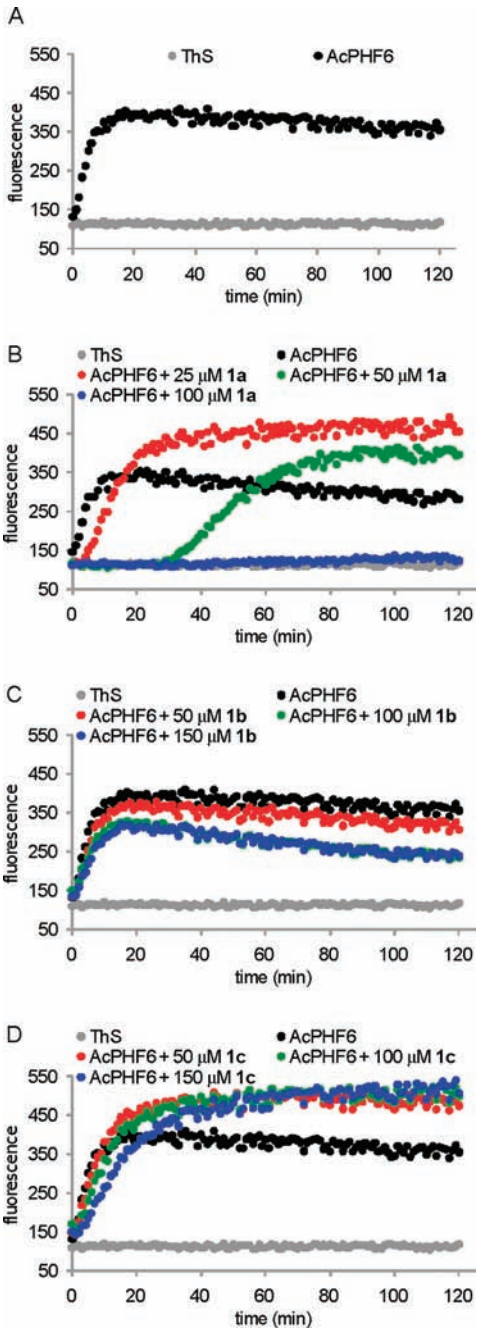

Figure 7. AcPHF6 aggregation and inhibition of AcPHF6 aggregation measured by ThS fluorescence. (A) Aggregation of 100 μM AcPHF6 (black) and ThS background fluorescence (gray). (B) Aggregation of 100 μM AcPHF6 in the absence and presence of 25, 50, and 100 μM macrocycle **1a**. (C) Aggregation of 100 μM AcPHF6 in the absence and presence of 50, 100, and 150 μM macrocycle **1b**. (D) Aggregation of 100 μM AcPHF6 in the absence and presence of 50, 100, and 150 μM macrocycle **1c**.

and R_2 residues. In macrocycle **1a**, the hydrophobic leucine residue is incorporated at R_7 to match the hydrophobic valine residue at R_1, and the hydrophilic lysine residue is incorporated at R_6 to match the polar glutamine residue at R_2. In macrocycle **1b**, the hydrophobic leucine residue is incorporated at R_6 to match the hydrophobic isoleucine residue at R_2, and the hydrophilic lysine residue is incorporated at R_7 to match the polar glutamine residue at R_1.

Figure 6 illustrates how macrocycles **1a** and **1b** are designed to bind the two edges of a growing AcPHF6 β-sheet and block further growth. The binding process should occur through parallel in-register β-sheet interactions, the same self-recognition process that drives the formation of AcPHF6 β-sheets. The molecular template Hao in the lower strand should block hydrogen-bonding interactions and thus block β-sheet growth. The *preorganized peptidic* structure of macrocycles **1a** and **1b** should complement the hydrogen-bonding groups of the edges of the AcPHF6 β-sheets, while providing an in-register orientation of like side chains and matching the pattern of hydrophobicity and hydrophilicity of the AcPHF6 side chains.

The effects of macrocycles **1a** and **1b** on AcPHF6 aggregation were studied with thioflavin S (ThS) fluorescence assays.[19,25] In these experiments, 100 μM AcPHF6 in 16 mM MOPS buffer is allowed to aggregate in the presence of ThS. ThS binds to the resulting aggregates and exhibits increasing fluorescence. The black curve in Figure 7A shows a typical experiment in which

dx.doi.org/10.1021/ja110545h | *J. Am. Chem. Soc.* 2011, 133, 3144–3157

AcPHF6 is allowed to aggregate without any added macrocycle and the fluorescence is monitored for 120 min. AcPHF6 aggregates immediately after it is added to the buffer with no observable lag time. The fluorescence signal in the black curve increases rapidly at first and saturates in about 20 min. The aggregation assays show some variation from experiment to experiment, as is common in such aggregation assays. For example, the fluorescence intensity at the saturation point varies slightly from experiment to experiment, and sometimes the fluorescence intensity decreases slightly at the end of an assay. For this reason, we performed each experiment in triplicate in 96-well plates and repeated experiments when appropriate to ensure reproducibility. Representative data from these experiments were selected for use in the figures. Examples of two independent experiments, each in triplicate, are provided in the Supporting Information (Figures S1 and S2).

Macrocycles **1a** and **1b** exhibit dramatic differences in their ability to inhibit the aggregation of AcPHF6. The VQIVY-KL macrocycle (**1a**) delays the onset of AcPHF6 aggregation in a concentration-dependent fashion (Figure 7B). In the presence of 25 μM **1a**, the aggregation of AcPHF6 is delayed. The red curve shows a lag time of about 5 min before the onset of rapid aggregation. The slope of the curve during the growth phase after 5 min is smaller than that of the black curve, which suggests slower aggregation. In the presence of 50 μM **1a**, the onset of AcPHF6 aggregation is delayed even more. The green curve shows a lag time of about 30 min, and the slope of the curve after 30 min is smaller than that of the red curve. In the presence of 100 μM **1a**, AcPHF6 aggregation is completely suppressed for the duration of the assay (120 min). The blue curve overlaps with the ThS background and shows no increase in the fluorescence signal.

Macrocycle **1a** causes an increase in fluorescence of the AcPHF6/ThS system at 25 and 50 μM. The increased fluorescence may arise from coaggregation of macrocycle **1a** with AcPHF6. It is also possible that macrocycle **1a** affects the conformation of the ThS dye and thus changes its fluorescence.[26] Other researchers have observed increased ThT fluorescence caused by the addition of other compounds in Aβ aggregation assays.[27] In one study, the number of Teflon mixing balls was shown to correlate with the intensity of ThT fluorescence in the aggregation of α-synuclein.[28] For these reasons, we have focused primarily on the effect of macrocycles **1** on the lag time rather than the fluorescence intensity.

The QIVYK-LK macrocycle (**1b**) shows no significant effect on AcPHF6 aggregation (Figure 7C). In the presence of 50, 100, and 150 μM **1b**, no lag time was observed in AcPHF6 aggregation. The slopes of the red, green, and blue curves are hardly changed compared with the slope of the black curve, which suggests that 50−150 μM **1b** does not change the rate of aggregation. Macrocycle **1b** causes a slight decrease in fluorescence of the AcPHF6/ThS system. The decreased fluorescence may result from stronger photobleaching of ThS in the presence of macrocycle **1b**, disaggregation of AcPHF6 fibrils, or a changed conformation of ThS.

The difference in inhibition by macrocycles **1a** and **1b** indicates that macrocycle **1a** interacts with the aggregating AcPHF6 and that either macrocycle **1b** does not interact with AcPHF6 or its interaction has no effect. Macrocycle **1b** is more hydrophilic than macrocycle **1a**, and this greater hydrophilicity may diminish its interactions with the aggregating AcPHF6. Specifically, macrocycle **1a** has a *hydrophobic* valine residue at the R_1 position, while macrocycle **1b** has a *hydrophilic* lysine residue at the R_5 position. It is also possible that macrocycle **1b** interacts with AcPHF6 but that the interaction has no effect on aggregation. Because macrocycles **1a** and **1b** are designed to bind the two different hydrogen-bonding edges of AcPHF6, the difference in inhibition raises the intriguing possibility that AcPHF6 β-sheets have a preferred direction of growth.[29] If this is the case, then macrocycle **1a** must inhibit aggregation by binding to the leading edge, which corresponds to the "green edge" in Figure 4.

2. Acyclic Controls 2a and 2b and Macrocyclic Controls 3a and 4a. We prepared two acyclic controls to test the importance of macrocyclic structures in blocking AcPHF6 aggregation: $^{\delta}$Orn-VQIVY-$^{\delta}$Orn-NH_2 (**2a**) and $^{\delta}$Orn-QIVYK-$^{\delta}$Orn-NH_2 (**2b**).

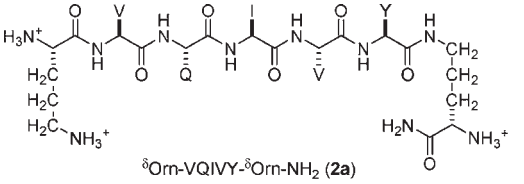

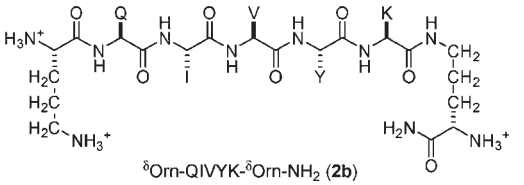

These two acyclic peptides lack the lower strands of macrocycles **1a** and **1b** and should not be able to adopt a preorganized β-sheet conformation. Neither of these acyclic peptides has an appreciable effect on the aggregation of AcPHF6. No lag in AcPHF6 aggregation occurs, and the slopes of the aggregation curves hardly change in the presence of these acyclic peptides (Figure 8). These results suggest that the lower strand in the macrocycle is important in blocking β-sheet interactions and that the preorganized β-sheet structure of the macrocycle is critical in recognizing the edges of AcPHF6 β-sheets.

We prepared two additional controls to explore the importance of the recognition strand and the preorganized β-sheet structure: *N*-methyl macrocycle **3a** and α-linked ornithine macrocycle **4a**, which are both mutants of the VQIVY-KL macrocycle (**1a**).

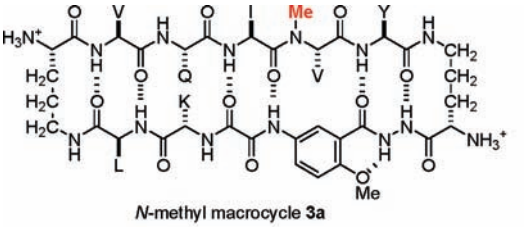

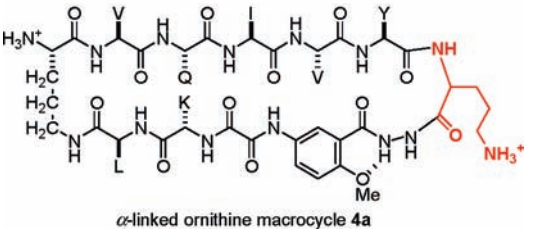

The *N*-methyl group on the R_4 valine in macrocycle **3a** disrupts the hydrogen-bonding ability of the upper strand. Macrocycle **3a** should not effectively bind to the edge of AcPHF6 β-sheets.[30] In macrocycle

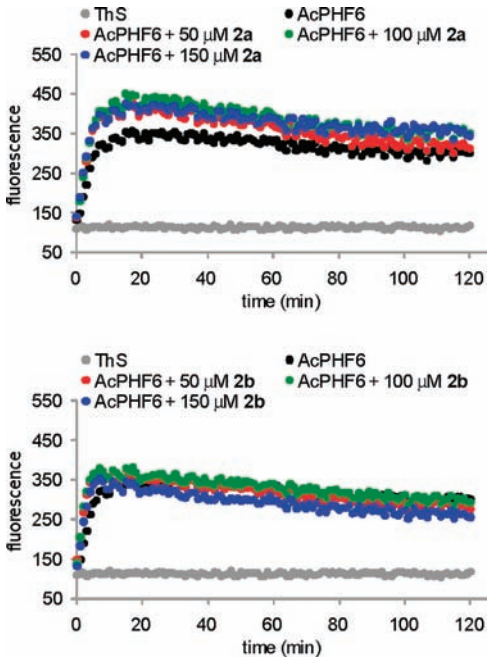

Figure 8. Aggregation of 100 μM AcPHF6 in the absence and presence of 50, 100, and 150 μM acyclic peptides **2a** and **2b**.

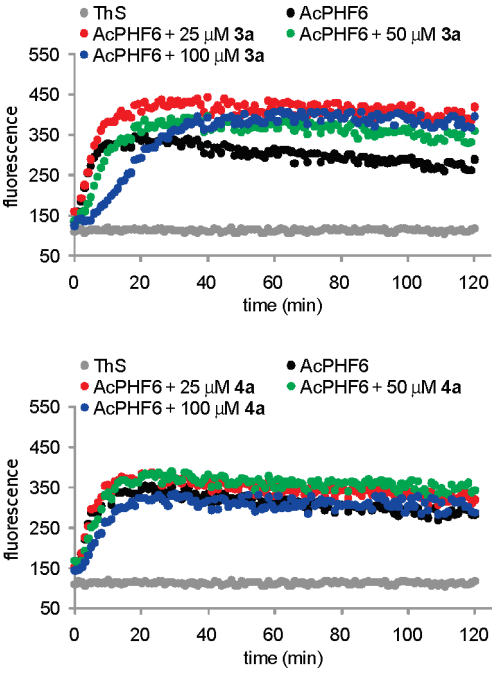

Figure 9. Aggregation of 100 μM AcPHF6 in the absence and presence of 25, 50, and 100 μM macrocycles **3a** and **4a**.

4a, the δ-linked ornithine on the right side is replaced with an α-linked ornithine, which should not mimic a β-turn and should disfavor a folded β-sheet structure.[31] These two controls exhibit diminished inhibition of AcPHF6 aggregation. Macrocycle **3a** slightly reduces the rate of AcPHF6 aggregation at 50 μM and also induces a small lag in aggregation at 100 μM; macrocycle **4a** slightly reduces the rate of AcPHF6 aggregation and induces a small lag at 100 μM (Figure 9). These observations are consistent with the binding model hypothesized in Figure 6 and highlight the importance of the potential of the macrocycles to adopt a preorganized β-sheet structure with an exposed hydrogen-bonding edge.

3. Macrocycles 1a and 1c and Macrocycles 1d, 1e, 1f, and 1g: Facial Hydrophobicity. We swapped the lysine and leucine side chains at the R_6 and R_7 positions of the VQIVY-KL macrocycle (**1a**) to test the effect of the hydrophobicity and hydrophilicity of the R_6 and R_7 side chains.

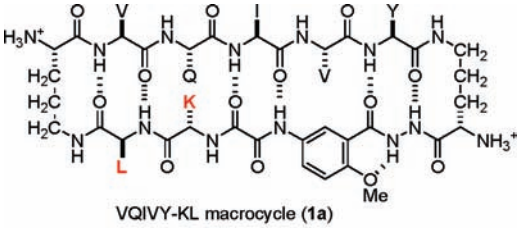

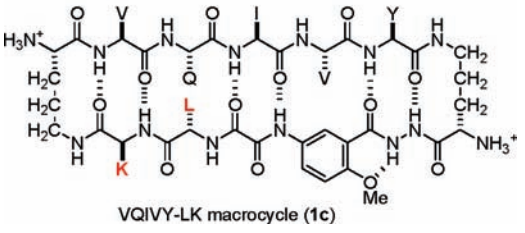

The resulting isomeric macrocycle VQIVY-LK (**1c**) maintains the upper (recognition) strand sequence and net 3+ charge but

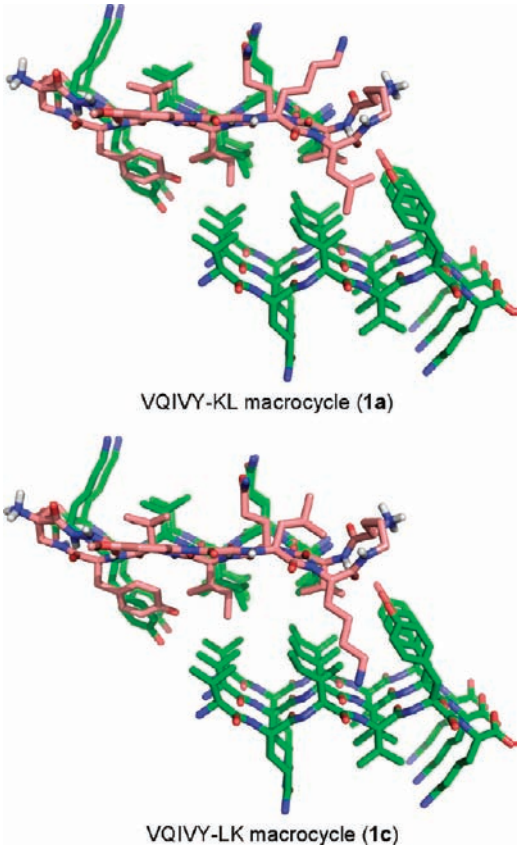

Figure 10. Models of macrocycles **1a** (top) and **1c** (bottom) bound to the edge of the antiparallel-layered parallel β-sheets formed by the VQIVYK peptide. The macrocycles are shown in pink, and the VQIVYK peptide strands are shown in green. The models were constructed by manually docking an energy-minimized model of macrocycle **1** (R_1—R_7 = CH_3) to the edges of VQIVYK[3b] in PyMOL and building the appropriate side chains.

dx.doi.org/10.1021/ja110545h |J. Am. Chem. Soc. 2011, 133, 3144–3157

places the hydrophilic lysine side chain at R_7 on the hydrophobic face formed by the R_1, R_3, and R_5 valine, isoleucine, and tyrosine. Macrocycle **1c** exhibits greatly diminished inhibition of AcPHF6 aggregation. In the presence of 50−150 μM **1c**, the rate of AcPHF6 aggregation is only slightly reduced (Figure 7D). The effects are small compared to those of macrocycle **1a**, in which a 25−100 μM concentration of the macrocycle results in progressively longer delays and suppression of aggregation.

The pronounced difference in inhibition by **1a** and **1c** is consistent with a model in which the macrocycles bind to the edges of the *layers* of antiparallel-layered parallel β-sheets. Figure 10 illustrates this binding model. Binding of macrocycle **1c** to the edge of AcPHF6 directs the hydrophilic lysine at the R_7 position inward into the hydrophobic pocket created by the isoleucine and tyrosine of the adjacent strand of AcPHF6, resulting in an unfavorable interaction. Conversely, the hydrophobic leucine at the R_7 position of macrocycle **1a** can fit snugly into this hydrophobic pocket. Thus, macrocycle **1a** binds more favorably to AcPHF6 β-sheets and inhibits AcPHF6 aggregation more strongly than macrocycle **1c**.

To corroborate the importance of facial hydrophobicity, we prepared the VQIVY-KV macrocycle (**1d**), the VQIVY-VK macrocycle (**1e**), the VQIVY-RL macrocycle (**1f**), and the VQIVY-LR macrocycle (**1g**).

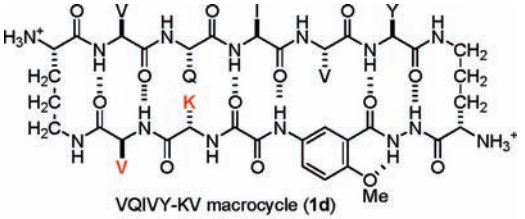

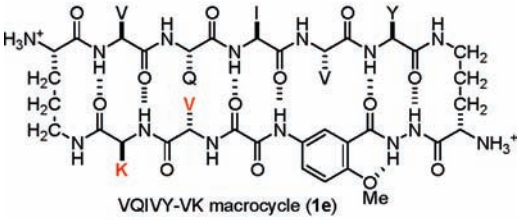

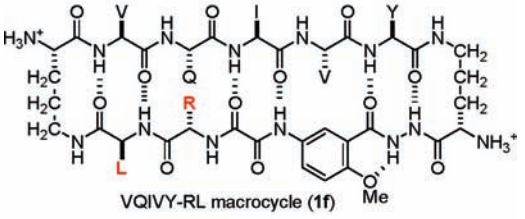

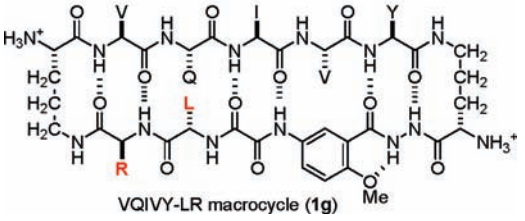

Macrocycle **1d** is a close homologue of macrocycle **1a** in which the leucine residue at the R_7 position is replaced with a valine residue; macrocycle **1f** is a close homologue of macrocycle **1a** in which the lysine residue at the R_6 position is replaced with an arginine residue. Like macrocycle **1a**, both **1d** and **1f** have a hydrophobic side chain at the R_7 position to match the facial hydrophobicity provided by the R_1, R_3, and R_5 side chains. On the other hand, macrocycles **1e** and **1g** are close homologues of macrocycle **1c** and have a hydrophilic side chain at the R_7 position.

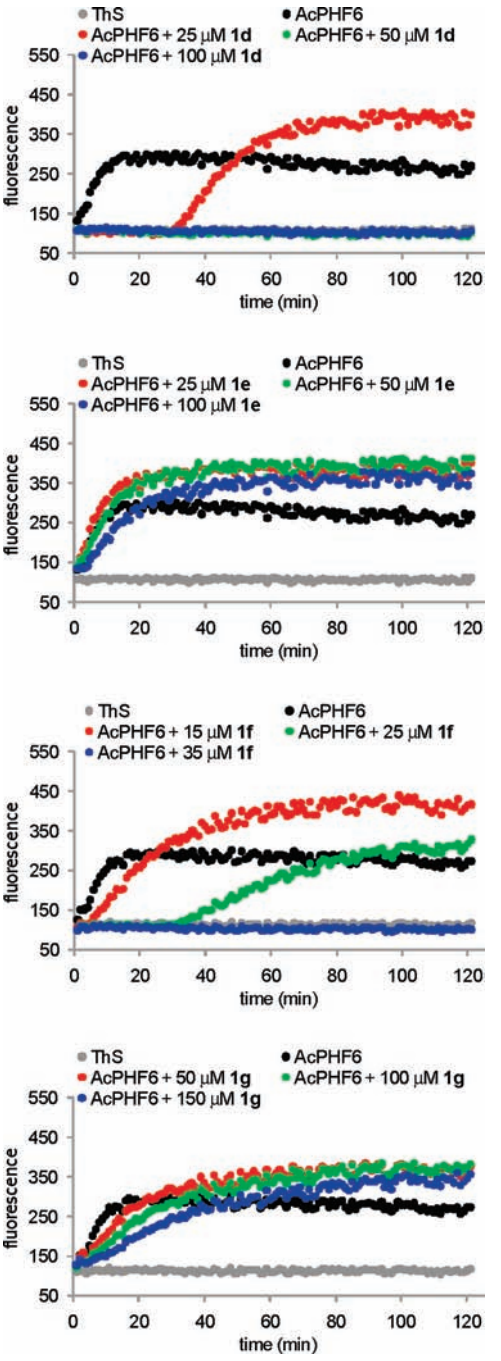

Figure 11. Aggregation of 100 μM AcPHF6 in the absence and presence of varying concentrations of macrocycles **1d**, **1e**, **1f**, and **1g**.

Like macrocycle **1a**, macrocycles **1d** and **1f** substantially delay and suppress the onset of AcPHF6 aggregation; like macrocycle **1c**, macrocycles **1e** and **1g** show little effect on AcPHF6 aggregation. Figure 11 illustrates the effects of varying concentrations of macrocycles **1d**, **1e**, **1f**, and **1g** on AcPHF6 aggregation. In the presence of 25 μM **1d**, the onset of AcPHF6

dx.doi.org/10.1021/ja110545h |*J. Am. Chem. Soc.* 2011, 133, 3144–3157

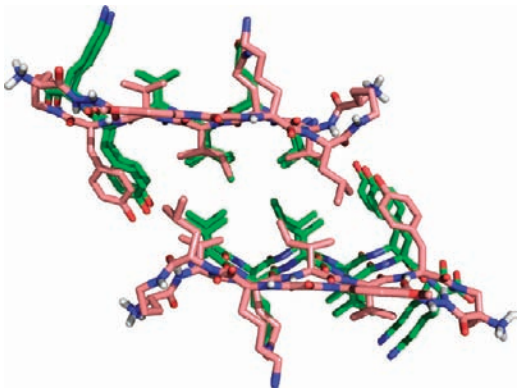

Figure 12. Model of two molecules of macrocycle **1a** cooperatively bound to the edge of the antiparallel-layered parallel β-sheets formed by the VQIVYK peptide. The macrocycles are shown in pink, and the VQIVYK peptide strands are shown in green. The model was constructed by manually docking two energy-minimized models of macrocycle **1** (R_1−R_7 = CH_3) to the edges of VQIVYK[3b] in PyMOL and building the appropriate side chains.

aggregation is delayed by about 30 min; 50 μM **1d** and 100 μM **1d** suppress AcPHF6 aggregation for the duration of the assay (120 min). In the presence of 25−100 μM **1e**, the rate of AcPHF6 aggregation is only slightly reduced. In the presence of 15 μM **1f**, the onset of AcPHF6 aggregation is delayed by about 5 min; 25 μM **1f** delays AcPHF6 aggregation by about 30 min; 35 μM **1f** suppresses AcPHF6 aggregation for the duration of the assay (120 min). In the presence of 25−100 μM **1g**, the rate of AcPHF6 aggregation is slightly reduced, in a concentration-dependent fashion. The substantial differences between **1d** and **1e** and between **1f** and **1g** corroborate the difference between **1a** and **1c** and thus emphasize the importance of a hydrophobic side chain at the R_7 position to match the facial hydrophobicity of the R_1, R_3, and R_5 side chains.

Macrocycles **1a**, **1d**, and **1f** show *nonlinear* effects of concentration on lag time. While 25 μM macrocycle **1a** gives a 5-min lag time, doubling the concentration of **1a** to 50 μM gives a 30-min lag time; further doubling the concentration of **1a** to 100 μM completely suppresses AcPHF6 aggregation for the duration of the assay, which indicates a lag time of no less than 120 min. While 25 μM macrocycle **1f** gives a 30-min lag time, slightly increasing the concentration of **1f** to 35 μM completely suppresses AcPHF6 aggregation for no less than 120 min.[32]

This nonlinear effect of concentration on lag time suggests that the inhibition is a cooperative process, in which two (or more) molecules of the macrocycle bind to the growing fibril or aggregate and block further growth. Figure 12 provides a model for this process. In this model, two molecules of **1a** bind to the antiparallel-layered parallel β-sheets of the VQIVYK peptide, forming a sandwich-like structure. The hydrophobic valine, isoleucine, tyrosine, and leucine groups at the R_1, R_3, R_5, and R_7 positions of macrocycle **1a** point inward to form a hydrophobic core. When the R_6 and R_7 residues are swapped, as in macrocycle **1c**, the hydrophilic lysine group at the R_7 position points inward, thus destabilizing the sandwich-like structure and preventing cooperativity.

4. Macrocycles 5a and 5c: Stereochemistry of R_6 and R_7. To further probe the effect of facial hydrophobicity at the R_6 and R_7 positions, we inverted the stereochemistry of the amino acids at these positions. Inversion of the stereochemistry

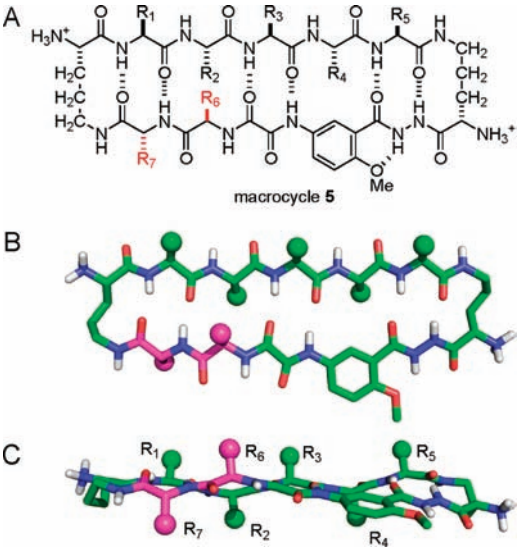

Figure 13. (A) Structure of macrocycle **5**. (B) Molecular model of macrocycle **5** (top view). (C) Molecular model of macrocycle **5** (side view) illustrating the facial positions of amino acid side chains R_1−R_7. The model is a minimum-energy conformer (local minimum) of the all-alanine analogue of macrocycle **5** (R_1−R_7 = CH_3) as calculated using Macromodel V6.5 with the MMFFs force field and GB/SA water solvation.

of the amino acids at R_6 and R_7 should direct the R_6 side chain onto the same face formed by the R_1, R_3, and R_5 side chains. Figure 13 illustrates this concept with a molecular model of macrocycle **5**, an analogue of macrocycle **1** with D-amino acids at R_6 and R_7. The amino acid side chain at R_6 points upward in the model of macrocycle **5**, while it points downward in the model of macrocycle **1** shown in Figure 3; the amino acid side chain at R_7 points downward in the model of macrocycle **5**, while it points upward in the model of macrocycle **1** shown in Figure 3.[33,34]

We prepared the VQIVY-dKdL macrocycle (**5a**) as a homologue of the VQIVY-KL macrocycle (**1a**), and the VQIVY-dLdK macrocycle (**5c**) as a homologue of the VQIVY-LK macrocycle (**1c**).

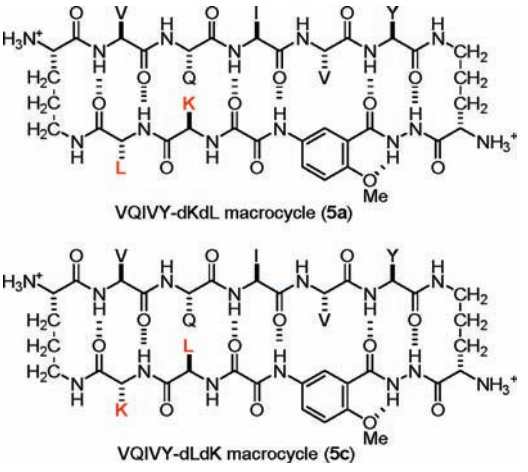

Macrocycle **5a** has the same sequence of amino acids as macrocycle **1a**, and the D-lysine side chain at the R_6 position is on the hydrophobic face formed by the R_1, R_3, and R_5 valine, isoleucine, and tyrosine. Macrocycle **5c** has the same sequence of amino acids as macrocycle **1c**, and the D-leucine side chain at the R_6

dx.doi.org/10.1021/ja110545h | *J. Am. Chem. Soc.* 2011, 133, 3144–3157

position is on the hydrophobic face formed by the R_1, R_3, and R_5 valine, isoleucine, and tyrosine.

Macrocycle **5c** is expected to have stronger inhibition of AcPHF6 aggregation because the D-leucine at the R_6 position matches the facial hydrophobicity provided by the valine, isoleucine, and tyrosine at the R_1, R_3, and R_5 positions, and these hydrophobic side chains can fit into the hydrophobic core formed by AcPHF6 β-sheets. The results are consistent with this hypothesis. Both macrocycles reduce the rate of AcPHF6 aggregation in a concentration-dependent fashion (Figure 14). Macrocycle **5c** shows a greater effect of reducing the rate of AcPHF6 aggregation than macrocycle **5a** at 25, 50, and 100 μM concentrations. These results further highlight the importance of facial hydrophobicity in molecular recognition of layered parallel β-sheets.

5. Structural Studies of Macrocycles 1 and 5. We performed X-ray crystallographic and solution-phase NMR studies to obtain structural information about macrocycles **1** and **5** in the solid state and in aqueous solution. To facilitate the X-ray crystallographic studies, we prepared brominated macrocycle **1h**.

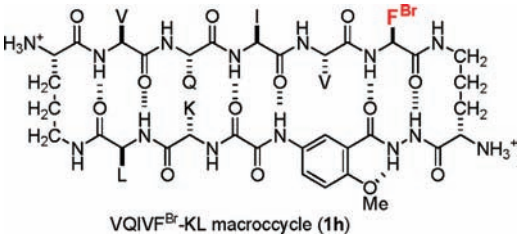

Macrocycle **1h** is a close homologue of the VQIVY-KL macrocycle (**1a**), in which the tyrosine (Y) residue at R_5 is replaced by 4-bromo-phenylalanine (F^{Br}). The bromine atom facilitates determining the phases in solving the crystal structure.[35] Figure 15 shows the crystal structure of macrocycle **1h**. The crystal structure reveals a macrocyclic β-sheet structure with a pattern of intramolecular hydrogen bonds similar to the molecular model of the alanine-based macrocycle **1** shown in Figure 3. The crystal structure differs slightly in conformation from the alanine-based model in that it is somewhat less flat and regular. The less regular structure may reflect side-chain interactions or crystal packing effects in **1h**.

^{1}H NMR studies of macrocycle **1a** and its homologue macrocycle **1c** establish that macrocycle **1c** is well-folded into a β-sheet structure and macrocycle **1a** is less well-folded into a β-sheet structure in aqueous solution. The macrocycles were studied at 2 mM in D_2O by TOCSY, ROESY, and one-dimensional ^{1}H NMR experiments. The NOE cross-peaks, α-proton chemical shifts, and $^{\delta}$Orn δ-proton magnetic anisotropy help elucidate the folding of the macrocycles.[20]

Characteristic NOE cross-peaks present in macrocycles **1a** and **1c** reflect the alignment of residues and proximities associated with a folded β-sheet structure (Figure 16). Both macrocycles show NOE cross-peaks between the proton at the 6-position of the aromatic ring of Hao and the α-proton of the R_4 valine. This long-range inter-residue NOE is one hallmark of β-sheet folding in these and related macrocycles.[20,36,37] Macrocycle **1c** also shows a cross-peak between the α-proton of the R_2 glutamine and the α-proton of the R_6 leucine. In macrocycle **1a**, a cross-peak between the α-proton of the R_2 glutamine and the α-proton of the R_6 lysine is not discernible. This cross-peak may be absent due to incomplete folding or may not be discernible in the

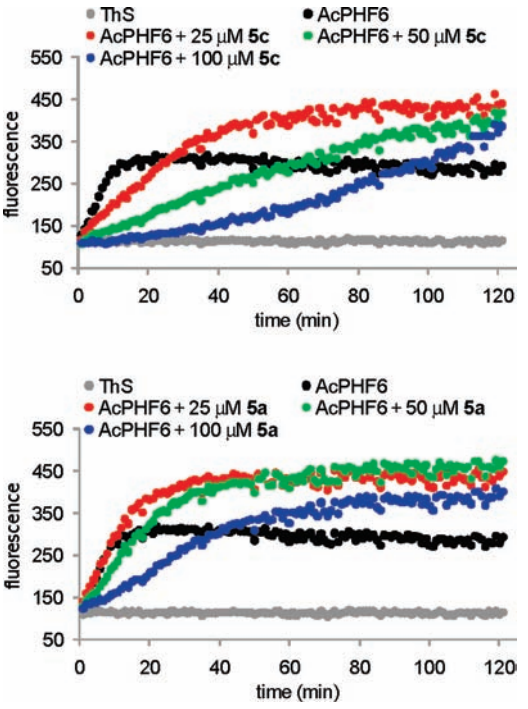

Figure 14. Aggregation of 100 μM AcPHF6 in the absence and presence of 25, 50, and 100 μM macrocycles **5a** and **5c**.

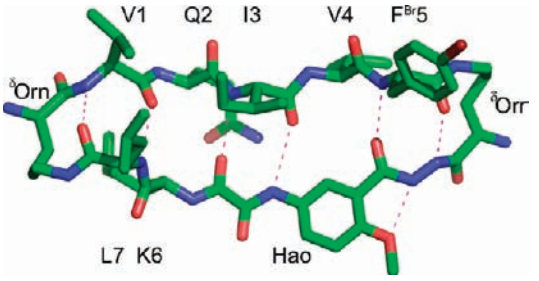

Figure 15. X-ray crystallographic structure of macrocycle **1h**. Intramolecular hydrogen bonds are shown as dashed lines.

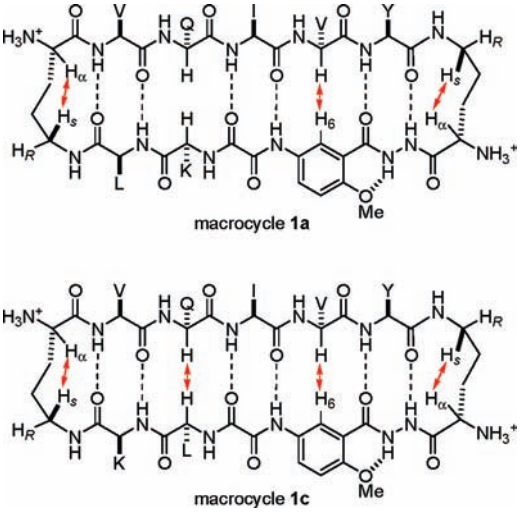

Figure 16. Key NOE cross-peaks observed in macrocycles **1a** and **1c**.

dx.doi.org/10.1021/ja110545h |*J. Am. Chem. Soc.* 2011, 133, 3144–3157

ROESY spectrum because the R_2 and R_6 resonances are close to each other and to the HOD peak. Macrocycle **1c** shows strong NOE cross-peaks between its ornithine α-protons and ornithine δ_S-protons, while these NOE cross-peaks are weaker in macrocycle **1a**. These results suggest that macrocycle **1c** is well-folded and that macrocycle **1a** is less well-folded.

Amino acid α-protons in a β-sheet conformation show downfield shifting compared with those in unstructured "random coil" conformations.[38] In related well-folded macrocycles, the α-protons of the amino acids in the upper strand exhibit a couple of tenths of a ppm downfield shifting, and less well-folded macrocycles exhibit more modest downfield shifting.[20] Because acyclic peptide **2a** should be largely unstructured, the chemical shifts of the α-protons of its V, Q, I, V, and Y amino acids provide reasonable context-specific "random coil" values. Both macrocycles **1a** and **1c** exhibit downfield shifting of the α-protons of the VQIVY pentapeptide strand, with the exception of the R_4 valine in **1a** (Figure 17). The downfield shifting of the residues in **1c** ranges from 0.06 to 0.36 ppm. These relatively substantial values are consistent with those that we have observed for related well-folded β-sheet structures.[20] Macrocycle **1a**, on the other hand, exhibits only modest downfield shifting. The α-protons of the R_1 valine, R_3 isoleucine, and R_5 tyrosine are shifted downfield by 0.03−0.20 ppm, while the glutamine α-proton is shifted downfield by only 0.01 ppm, and the α-proton of the R_4 valine is shifted upfield by 0.02 ppm. These values are consistent with those that we have seen for less well-folded β-sheet structures.[20]

The magnetic anisotropy of the diastereotopic $^{\delta}$Orn δ-protons ($\Delta\delta^{\delta}$Orn) provides an additional measure of the degree of β-sheet folding. We have previously observed that a $^{\delta}$Orn δ-proton magnetic anisotropy of ca. 0.6 ppm corresponds to complete β-sheet folding in water for related macrocycles.[20] Acyclic peptide **2a** exhibits $\Delta\delta^{\delta}$Orn values of 0.00 and 0.03 ppm, indicating essentially no folding of the ornithine units. Macrocycle **1a** exhibits $\Delta\delta^{\delta}$Orn values that are both 0.20 ppm, indicating partial folding of the turn units. Macrocycle **1c** exhibits $\Delta\delta^{\delta}$Orn values of 0.52 and 0.42 ppm, indicating better folding of the turn units (Table 1).

^{1}H NMR studies establish well-folded β-sheet structures for macrocycles **1b**, **1e**, and **1g** and less well-folded β-sheet structures for macrocycles **1d** and **1f** (Figure 17 and Table 1). The downfield shifting of the α-protons and the $^{\delta}$Orn δ-proton magnetic anisotropy show that the VQIVY-VK macrocycle (**1e**) is not as well-folded as the VQIVY-LK macrocycle (**1c**) but is still largely folded. The downfield shifting of the α-protons and the $^{\delta}$Orn δ-proton magnetic anisotropy show that the VQIVY-LR macrocycle (**1g**) is slightly better folded than macrocycle **1c**. It is worth noting that the well-folded macrocycles **1c**, **1e**, and **1g** are close homologues and have hydrophilic side chains at the R_7 position. Macrocycles **1a**, **1d**, and **1f** are close homologues and have hydrophobic side chains at the R_7 position. Like macrocycle **1a**, macrocycles **1d** and **1f** are less well-folded. The D-amino acid mutants **5a** and **5c** are less well-folded, perhaps because the inverted stereochemistry compromises the β-sheet conformation.

It is interesting that the best inhibitors are not the best folded. Macrocycles **1a**, **1d**, and **1f** substantially delay aggregation at 25−50 μM and completely suppress it at 35−100 μM, although their α-proton chemical shifts and $^{\delta}$Orn δ-proton magnetic anisotropy are substantially less than those of well-folded macrocycles **1c**, **1e**, and **1g**. Although macrocycles **1a**, **1d**, and **1f** are not completely preorganized in aqueous solution, they should be able to adopt a β-sheet conformation as part of a dynamic process. The crystal structure of macrocycle **1h** suggests that these homologous macrocycles can adopt a β-sheet conformation in the solid state, and it is likely that they can also adopt such a conformation upon binding to growing AcPHF6 aggregates. What is common to all three of these macrocycles is that the hydrophobic side chain at the R_7 position matches the facial hydrophobicity provided by the R_1, R_3, and R_5 side chains.

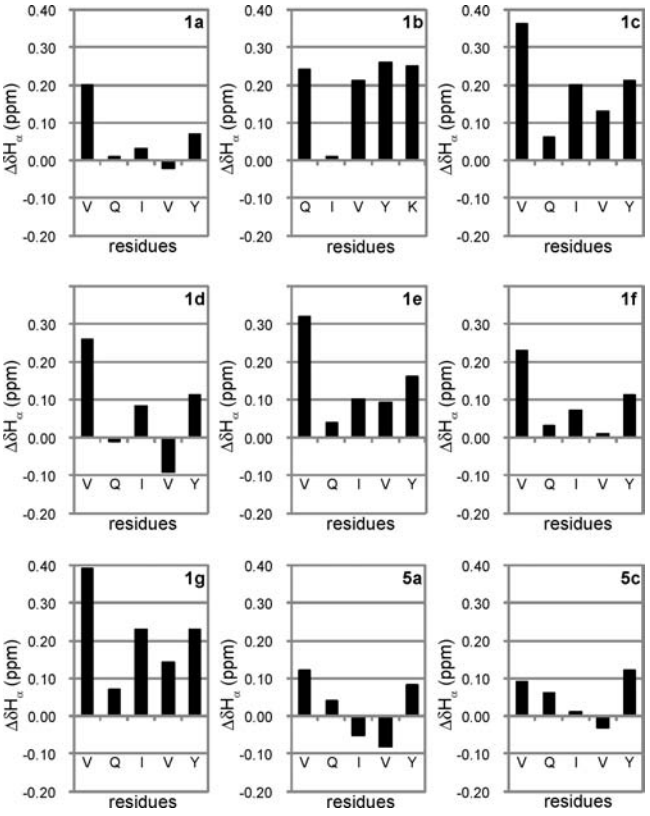

Figure 17. Downfield shifting of the α-protons of macrocycles **1** and **5** relative to those of acyclic peptides **2a** or **2b** ($\Delta\delta H_\alpha$ = macrocycle δH_α − acyclic control δH_α). NMR data were collected at 2 mM in D_2O at 298 K.

Table 1. Magnetic Anisotropy of the δ-Linked Ornithines of Macrocycles 1a−1g, Acyclic Peptides 2a and 2b, and Macrocycles 5a and 5c[a]

	magnetic anisotropy (ppm)	
peptide	$^{\delta}$Orn(1)[b]	$^{\delta}$Orn(2)[b]
1a	0.20	0.20
1b	0.58	0.52
1c	0.52	0.42
1d	0.27	0.27
1e	0.43	0.32
1f	0.22	0.22
1g	0.55	0.43
2a	0.00	0.03
2b	0.00	0.00
5a	0.20	0.16
5c	0.27	0.08

[a] NMR data were collected at 2 mM in D_2O at 298 K. [b] The assignment of $^{\delta}$Orn(1) and $^{\delta}$Orn(2) is arbitrary.

dx.doi.org/10.1021/ja110545h | J. Am. Chem. Soc. 2011, 133, 3144–3157

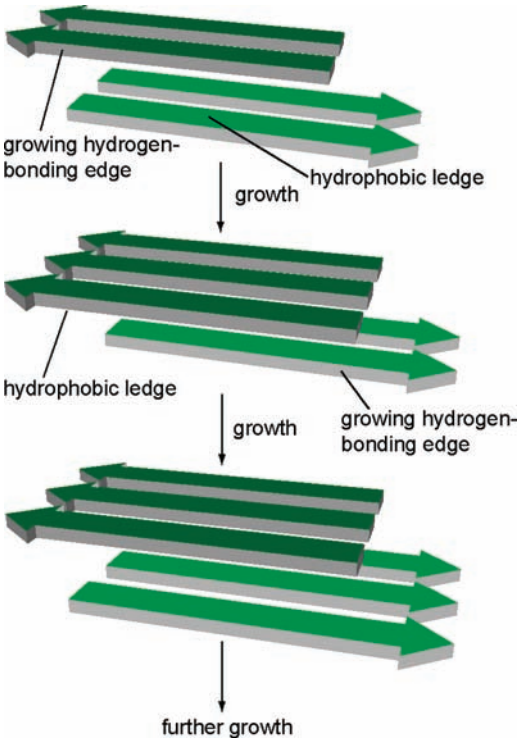

Figure 18. Layered-growth model of AcPHF6 β-sheets.

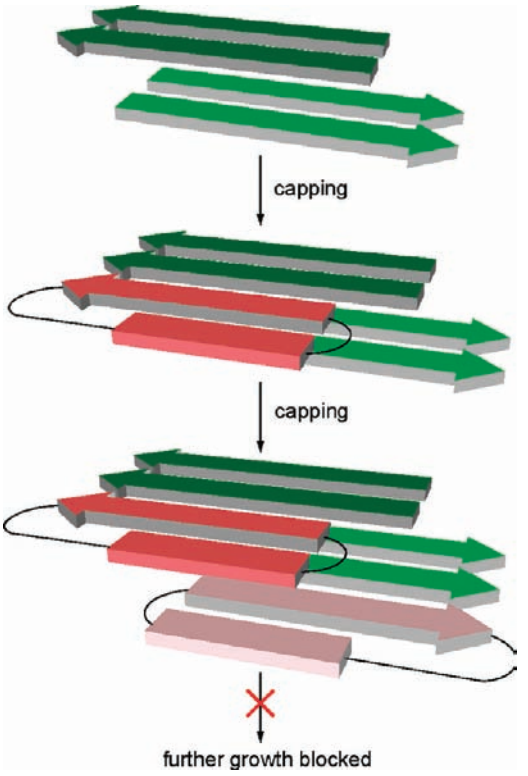

Figure 19. Inhibition of layered growth by macrocycles.

6. Model of AcPHF6 Growth and Inhibition. The binding model put forth in Figure 12 elucidates widespread but underappreciated targets in β-sheet aggregation—the paired edges of antiparallel-layered parallel β-sheets. The substantially different inhibition by macrocycles with a different recognition sequence (**1a** and **1b**) or different hydrophobicity of the R_7 side chain (**1a** and **1c**) and the nonlinear effect of concentration on lag time all provide insights into the growth mechanism of layered β-sheets. On the basis of these results and the crystal structure of VQIVYK, we envision a model of AcPHF6 β-sheet growth in which the layers in a pair of layered β-sheets do not grow separately but rather grow concurrently by adding peptide strands alternately to each layer. Figure 18 illustrates this model with a cartoon.

In this *layered-growth model*, the layered β-sheets grow by alternately adding peptide strands to the top and bottom layers. The peptide strands of the top and bottom layers are staggered with respect to each other, creating a hydrophobic ledge and a hydrogen-bonding edge that is partially shielded from bulk water by the ledge. Growth occurs by docking a new peptide strand to the ledge through hydrophobic interactions and to the edge through hydrogen-bonding interactions. The addition of the new peptide strand creates a new hydrophobic ledge and a new hydrogen-bonding edge in the other layer that is partially shielded from bulk water, thus promoting further growth. This combination of hydrophobic interactions and hydrogen bonding provides a molecular recognition motif that is reminiscent of *overhangs* in DNA ligation.

An important feature of the antiparallel-layered parallel β-sheets of VQIVYK is that the hydrogen-bonding edge at the "front" of the layer differs from the hydrogen-bonding edge at the "back" of the layer. Although the "front" and "back" of the layer both present hydrogen-bonding edges and hydrophobic ledges, the hydrogen-bonding edge at the "front" presents different hydrogen-bonding amino acids from those at the "back". On the "front" edge, the V, I, and Y amino acids present hydrogen-bonding groups; on the "back" edge, the Q, V, and K amino acids present hydrogen-bonding groups. For this reason, growth by addition of peptide strands to the "front" and "back" edges is nonequivalent, and there is a preferred direction of growth.[29] Because such antiparallel-layered parallel β-sheets occur widely in amyloid structures,[1−7] this model of growth is likely applicable to other amyloid β-sheets.[39]

The macrocycles inhibit the layered growth by cooperatively capping the leading "front" edge of the β-sheet layer through the same sorts of hydrophobic and hydrogen-bonding interactions that are involved in β-sheet growth. Inhibition occurs by docking the macrocycle to the hydrophobic ledge and hydrogen-bonding edge of the growing antiparallel-layered parallel β-sheet. The addition of the macrocycle to one layer creates a new hydrophobic ledge and a new hydrogen-bonding edge in the other layer that is partially shielded from bulk water. Addition of a second macrocycle to this ledge and edge completes the capping and prevents further growth, as the Hao templates block additional hydrogen-bonding interactions.

Growing β-sheets in amyloid aggregation have been popular targets for inhibitor design, and researchers have designed different types of inhibitors aimed at the hydrogen-bonding edges of β-sheets.[40] Among these inhibitors are peptides containing *N*-methylated amino acids,[41] α,α-disubstituted amino acids,[42] amide-to-ester backbone modification,[43] and β-sheet-breaking prolines.[44] What is unique about the models of growth in Figure 18 and inhibition in Figure 19 is that they involve the growth of two layers of β-sheets in concert and inhibition by cooperative binding to both of these layers. Although the binding is almost certainly reversible, more potent and possibly irreversible inhibitors that target both layers at once can be envisioned.

dx.doi.org/10.1021/ja110545h | *J. Am. Chem. Soc.* 2011, 133, 3144–3157

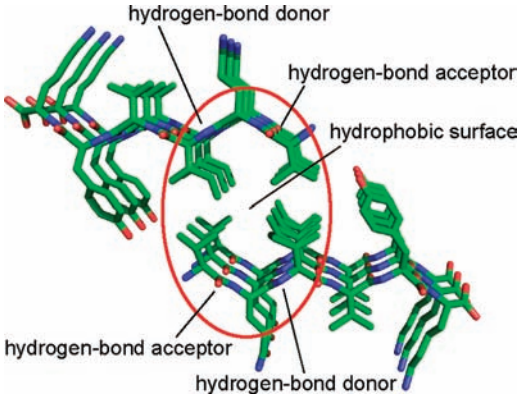

Figure 20. The paired edges of the antiparallel-layered parallel β-sheets of tau-derived peptide VQIVYK[3b] as a target for inhibitor design.

The commonality of antiparallel-layered parallel β-sheets in amyloid aggregation opens a new direction for inhibitor design, perhaps not only for peptidic inhibitors but also for small molecules. Figure 20 illustrates a potential target for small-molecule inhibitors. The target contains multiple hydrogen-bond donors, hydrogen-bond acceptors, and a hydrophobic surface. There is now considerable interest in amyloid oligomers as the toxic species in amyloid aggregation.[45−49] Although the structures of these oligomers are only beginning to be elucidated, their formation likely involves the formation of hydrogen-bonded β-sheets that are reinforced through layered hydrophobic buttressing.[50−52] For these reasons, the design of inhibitors that target the edges of layered β-sheets is likely to be of broad importance in drug discovery in neurodegenerative diseases.

CONCLUSIONS

We have developed a series of macrocycles with suitable recognition strands and facial hydrophobicity that delay and suppress the onset of aggregation of AcPHF6. The substantial difference in inhibition by the VQIVY-KL macrocycle (**1a**) and the QIVYK-LK macrocycle (**1b**) suggests the possibility of a preferred direction of AcPHF6 β-sheet growth. The substantial difference in inhibition by the VQIVY-KL macrocycle (**1a**) and the VQIVY-LK macrocycle (**1c**) demonstrates that a hydrophobic side chain at the R_7 position to match the facial hydrophobicity provided by the R_1, R_3, and R_5 side chains is critical in recognition between the AcPHF6 layered β-sheets and the macrocycles. Results from macrocycles **1d**, **1e**, **1f**, and **1g** and macrocycles **5a** and **5c** further highlight this point. The nonlinear effect of concentration on lag time suggests cooperative inhibition by macrocycle **1a** and also by its analogues **1d** and **1f**. This cooperative inhibition is consistent with a binding model in which two molecules of the macrocycle bind simultaneously to the two β-sheet layers of VQIVYK. On the basis of these results and the crystal structure of VQIVYK, we envision a model of AcPHF6 growth in which the two layers of the layered β-sheets grow concurrently by adding peptide strands alternately to each layer. The macrocycles inhibit β-sheet growth by cooperatively binding to these two layers. This model of growth and inhibition opens a provocative and appealing target for future inhibitor design in amyloid aggregation—the paired edges of antiparallel-layered parallel β-sheets.

These studies of the AcPHF6 model system may provide insights for the design of inhibitors of tau protein aggregation. The recent failure of Aβ-focused therapeutic agents in phase III clinical trials further underlines the importance of developing alternative drug design approaches for Alzheimer's disease.[53] Tau is an attractive alternative target. In searching for tau aggregation inhibitors, researchers have focused mostly on screening libraries of compounds.[54,55] The principles elucidated through these studies of the AcPHF6 model system should be useful in guiding the specific design of peptidic and small-molecule inhibitors that target the paired edges of layered β-sheets in tau aggregation, as well as other β-sheet amyloids in a variety of neurodegenerative diseases.

EXPERIMENTAL SECTION

Sample Preparation. Macrocycles **1**, **4a**, and **5** and acyclic peptides **2** were synthesized and purified as described previously.[20] All peptides were characterized by electrospray mass spectrometry, analytical RP-HPLC, one-dimensional ^{1}H NMR spectroscopy, and TOCSY NMR experiments. Macrocycles **1a** and **1c** were also characterized by ROESY NMR experiments. NMR experiments were performed on 2 mM solutions in D_2O. Each peptide showed suitable purity, with a single sharp peak in the analytical RP-HPLC, appropriate peaks in the mass spectra associated with molecular ions, and well-dispersed and sharp peaks in the NMR spectra. The *N*-methyl macrocycle **3a** was synthesized in a similar fashion to macrocycles **1**, except that in the solid-phase synthesis of the linear precursor, Fmoc-Ile-OH (3 equiv) was coupled manually with HATU (3 equiv), HOAt (3 equiv), and DIEA (6 equiv) in NMP (triple coupling, 1.5 h per coupling).[56] AcPHF6 (Ac-VQIVYK-NH_2) was synthesized on Rink amide resin using Fmoc-based chemistry with HCTU and collidine and was acetylated with acetic anhydride and pyridine and purified as described previously.[19a]

ThS Fluorescence Assays of AcPHF6 Aggregation. ThS fluorescence assays were performed as described previously with minor variations.[19a] Stock solutions of ThS (A), peptide inhibitors (B), and AcPHF6 (C) were prepared beforehand as follows: (A) 0.5 mg/mL ThS solution in 20 mM MOPS buffer (pH 7.2) containing 0.01% NaN_3; the pH of the MOPS buffer was adjusted using a 1 M NaOH solution and a pH meter; (B) 1.0 mM solutions of the peptide inhibitors in pure H_2O; (C) 1.0 mM AcPHF6 solution in pure H_2O. Stock solutions B and C were prepared by weighing an appropriate amount of peptide and adding a corresponding volume of pure H_2O to make a 1.0 mM solution. All peptides were assumed to be TFA salts in which each free amino group is protonated and bears a $CF_3CO_2^-$ counterion.[57] The ThS fluorescence assays were conducted in standard 96-well plates (96-well optical clear bottom plate, black, polymer base, NUNC, USA). A typical assay plate comprises ThS control wells, inhibitor control wells, AcPHF6 control wells, and wells that contain AcPHF6 and various concentrations of inhibitors. The wells were prepared in triplicate or greater, and representative data were selected for further analysis. To each ThS control well were added 20 μL of stock solution A, 140 μL of 20 mM pH 7.2 MOPS buffer, and 40 μL of pure H_2O. To each inhibitor control well were added 20 μL of stock solution A, 140 μL of 20 mM pH 7.2 MOPS buffer, 20 μL of stock solution B, and 20 μL of pure H_2O. To each AcPHF6 control well were added 20 μL of stock solution A, 140 μL of 20 mM pH 7.2 MOPS buffer, 20 μL of pure H_2O, and finally at the very end of preparing the plate 20 μL of stock solution C. To each AcPHF6/inhibitor well were added 20 μL of stock solution A, 140 μL of 20 mM pH 7.2 MOPS buffer, different volumes (5−20 μL) of stock solution B to make an appropriate final concentration of the inhibitor, 0−15 μL of pure H_2O to bring the total volume to 180 μL, and finally at the very end of preparing the plate 20 μL of stock solution C. The total reaction volume in each well was 200 μL, and the final concentration of MOPS buffer in each well was 16 mM. No mixing balls were used in the wells.[58] After the plate was prepared, it was sealed quickly with adhesive film

dx.doi.org/10.1021/ja110545h | *J. Am. Chem. Soc.* 2011, 133, 3144–3157

(VWR), and the fluorescence assay was immediately begun. The assay was conducted in a Gemini XPS fluorescence plate reader (Molecular Devices, Sunnyvale, CA) at 25−27 °C with excitation and emission wavelengths at 440 and 490 nm, respectively. Fluorescence data were recorded every minute over 120 min with continuous shaking between each reading.

■ ASSOCIATED CONTENT

Supporting Information. Complete ref 50; examples of two independent experiments associated with Figure 7B; details of NMR experiments; chemical shifts of the α-protons of macrocycles **1** and **5** and acyclic peptides **2**; and NMR spectra (1D, TOCSY, and ROESY) of macrocycles **1a** and **1c**. This material is available free of charge via the Internet at http://pubs.acs.org.

■ AUTHOR INFORMATION

Corresponding Author
jsnowick@uci.edu

■ ACKNOWLEDGMENT

J.S.N. and J.Z. thank the National Institutes of Health (GM-49076) for grant support. D.E. and M.R.S. thank the HHMI and National Institutes of Health (AG-029430). S.K. thanks the Pakistan Higher Education Commission for fellowship support.

■ REFERENCES

(1) (a) Tycko, R. *Curr. Opin. Struct. Biol.* **2004**, *14*, 96–103. (b) Petkova, A. T.; Yau, W. M.; Tycko, R. *Biochemistry* **2006**, *45*, 498–512. (c) Paravastu, A. K.; Leapman, R. D.; Yau, W. M.; Tycko, R. *Proc. Natl. Acad. Sci. U.S.A.* **2008**, *105*, 18349–18354. (d) Luca, S.; Yau, W. M.; Leapman, R.; Tycko, R. *Biochemistry* **2007**, *46*, 13505–13522.

(2) (a) Lührs, T.; Ritter, C.; Adrian, M.; Riek-Loher, D.; Bohrmann, B.; Döbeli, H.; Schubert, D.; Riek, R. *Proc. Natl. Acad. Sci. U.S.A.* **2005**, *102*, 17342–17347. (b) Ritter, C.; Maddelein, M. L.; Siemer, A. B.; Lührs, T.; Ernst, M.; Meier, B. H.; Saupe, S. J.; Riek, R. *Nature* **2005**, *435*, 844–848. (c) Vilar, M.; Chou, H. T.; Lührs, T.; Maji, S. K.; Riek-Loher, D.; Verel, R.; Manning, G.; Stahlberg, H.; Riek, R. *Proc. Natl. Acad. Sci. U.S.A.* **2008**, *105*, 8637–8642.

(3) (a) Nelson, R.; Sawaya, M. R.; Balbirnie, M.; Madsen, A. Ø.; Riekel, C.; Grothe, R.; Eisenberg, D. *Nature* **2005**, *435*, 773–778. (b) Sawaya, M. R.; Sambashivan, S.; Nelson, R.; Ivanova, M. I.; Sievers, S. A.; Apostol, M. I.; Thompson, M. J.; Balbirnie, M.; Wiltzius, J. J.; McFarlane, H. T.; Madsen, A. Ø.; Riekel, C.; Eisenberg, D. *Nature* **2007**, *447*, 453–457. (c) Wiltzius, J. J.; Sievers, S. A.; Sawaya, M. R.; Cascio, D.; Popov, D.; Riekel, C.; Eisenberg, D. *Protein Sci.* **2008**, *17*, 1467–1474. (d) Ivanova, M. I.; Sievers, S. A.; Sawaya, M. R.; Wall, J. S.; Eisenberg, D. *Proc. Natl. Acad. Sci. U.S.A.* **2009**, *106*, 18990–18995.

(4) Shivaprasad, S.; Wetzel, R. *Biochemistry* **2004**, *43*, 15310–15317.

(5) Madine, J.; Copland, A.; Serpell, L. C.; Middleton, D. A. *Biochemistry* **2009**, *48*, 3089–3099.

(6) van der Wel, P. C. A.; Lewandowski, J. R.; Griffin, R. G. *J. Am. Chem. Soc.* **2007**, *129*, 5117–5130.

(7) Walsh, P.; Simonetti, K.; Sharpe, S. *Structure* **2009**, *17*, 417–426.

(8) Chiti, F.; Dobson, C. M. *Annu. Rev. Biochem.* **2006**, *75*, 333–366.

(9) (a) Garcia, M. L.; Cleveland, D. W. *Curr. Opin. Cell Biol.* **2001**, *13*, 41–48. (b) Trojanowski, J. Q.; Lee, V. M. *Nat. Neurosci.* **2005**, *8*, 1136–1137. (c) Ballatore, C.; Lee, V. M.; Trojanowski, J. Q. *Nat. Rev. Neurosci.* **2007**, *8*, 663–672.

(10) (a) Gustke, N.; Trinczek, B.; Biernat, J.; Mandelkow, E. M.; Mandelkow, E. *Biochemistry* **1994**, *33*, 9511–9522. (b) Mandelkow, E. M.; Biernat, J.; Drewes, G.; Gustke, N.; Trinczek, B.; Mandelkow, E. *Neurobiol. Aging* **1995**, *16*, 355–363. (c) Mandelkow, E. M.; Mandelkow, E. *Trends Cell Biol.* **1998**, *8*, 425–427. (d) Mandelkow, E.; von Bergen, M.; Biernat, J.; Mandelkow, E. M. *Brain Pathol.* **2007**, *17*, 83–90.

(11) von Bergen, M.; Friedhoff, P.; Biernat, J.; Heberle, J.; Mandelkow, E. M.; Mandelkow, E. *Proc. Natl. Acad. Sci. U.S.A.* **2000**, *97*, 5129–5134.

(12) Alternative models of related peptides based on low-resolution fiber and powder diffraction data have also been published:Inouye, H.; Sharma, D.; Goux, W. J.; Kirschner, D. A. *Biophys. J.* **2006**, *90*, 1774–1789.

(13) Margittai, M.; Langen, R. *Proc. Natl. Acad. Sci. U.S.A.* **2004**, *101*, 10278–10283.

(14) Coordinates of the STAG(−2) model were provided by Dr. Robert Tycko.

(15) DeLano, W. L. *The PyMOL Molecular Graphics System* DeLano Scientific: San Carlos, CA, 2002.

(16) In some other amyloids, contacts between polar residues such as glutamine and asparagine can play important roles in the face-to-face packing interaction between layered β-sheets.[3a] Antiparallel β-sheets can also form layered amyloid structures, and different face-to-face packing modes can occur.[3b]

(17) Amino acid residues in peptide names and amino acid side chains in chemical structures are both designated with the standard one-letter codes for natural amino acids, for example, V for valine, Q for glutamine, K for lysine, etc.

(18) Small peptides have been used as models in studies of the aggregation of other biologically relevant peptides or proteins. The limited conformational polymorphism of these model systems offers an advantage of greater simplicity than the full-length peptides or proteins. (a) Lanning, J. D.; Hawk, A. J.; Derryberry, J.; Meredith, S. C. *Biochemistry* **2010**, *49*, 7108–7118. (b) Mehta, A. K.; Lu, K.; Childers, W. S.; Liang, Y.; Dublin, S. N.; Dong, J. J.; Snyder, J. P.; Pingali, S. V.; Thiyagarajan, P.; Lynn, D. G. *J. Am. Chem. Soc.* **2008**, *130*, 9829–9835. (c) Liang, Y.; Lynn, D. G.; Berland, K. M. *J. Am. Chem. Soc.* **2010**, *132*, 6306–6308.

(19) (a) Goux, W. J.; Kopplin, L.; Nguyen, A. D.; Leak, K.; Rutkofsky, M.; Shanmuganandam, V. D.; Sharma, D.; Inouye, H.; Kirschner, D. A. *J. Biol. Chem.* **2004**, *279*, 26868–26875. (b) Rojas Quijano, F. A.; Morrow, D.; Wise, B. M.; Brancia, F. L.; Goux, W. J. *Biochemistry* **2006**, *45*, 4638–4652.

(20) Woods, R. J.; Brower, J. O.; Castellanos, E.; Hashemzadeh, M.; Khakshoor, O.; Russu, W. A.; Nowick, J. S. *J. Am. Chem. Soc.* **2007**, *129*, 2548–2558.

(21) Nowick, J. S.; Chung, D. M.; Maitra, K.; Maitra, S.; Stigers, K. D.; Sun, Y. *J. Am. Chem. Soc.* **2000**, *122*, 7654–7661. The molecular template is called "Hao" because it comprises hydrazine, 5-amino-2-methoxybenzoic acid, and oxalic acid groups.

(22) Nowick, J. S.; Lam, K. S.; Khasanova, T. V.; Kemnitzer, W. E.; Maitra, S.; Mee, H. T.; Liu, R. *J. Am. Chem. Soc.* **2002**, *124*, 4972–4973.

(23) Nowick, J. S.; Brower, J. O. *J. Am. Chem. Soc.* **2003**, *125*, 876–877.

(24) The macrocycles are named with the one-letter codes for residues at the R_1−R_7 positions.

(25) Friedhoff, P.; Schneider, A.; Mandelkow, E. M.; Mandelkow, E. *Biochemistry* **1998**, *37*, 10223–10230.

(26) Wolfe, L. S.; Calabrese, M. F.; Nath, A.; Blaho, D. V.; Miranker, A. D.; Xiong, Y. *Proc. Natl. Acad. Sci. U.S.A.* **2010**, *107*, 16863–16868.

(27) (a) Orner, B. P.; Liu, L.; Murphy, R. M.; Kiessling, L. L. *J. Am. Chem. Soc.* **2006**, *128*, 11882–11889. (b) Hudson, S. A.; Ecroyd, H.; Kee, T. W.; Carver, J. A. *FEBS J.* **2009**, *276*, 5960–5972.

(28) Pronchik, J.; He, X. L.; Giurleo, J. T.; Talaga, D. S. *J. Am. Chem. Soc.* **2010**, *132*, 9797–9803.

(29) A preferred direction of growth has also been observed in amyloid fibrils of $A\beta_{1-40}$ and insulin:(a) Ban, T.; Hoshino, M.; Takahashi, S.; Hamada, D.; Hasegawa, K.; Naiki, H.; Goto, Y. *J. Mol. Biol.* **2004**, *344*, 757–767. (b) Ban, T.; Yamaguchi, K.; Goto, Y. *Acc. Chem. Res.* **2006**, *39*, 663–670. (c) Heldt, C. L.; Zhang, S.; Belfort, G. *Proteins: Struct., Funct., Bioinf.* **2010**, *79*, 92–98.

(30) Attempts to synthesize a double *N*-methyl macrocycle with *N*-methyl groups on R_2 glutamine and R_4 valine proved unsuccessful.

(31) We initially designed a double α-ornithine macrocycle in which both δ-linked ornithines are replaced by α-linked ornithines, but we encountered difficulty in cyclization.

(32) Both macrocycles **1d** and **1f** suppress AcPHF6 aggregation for the duration of the assay (120 min) at substoichiometric concentrations. To test if macrocycle **1a** can suppress AcPHF6 aggregation at substoichiometric concentrations, we conducted an assay of 200 μM AcPHF6 in the presence of 25, 50, and 100 μM macrocycle **1a**. AcPHF6 aggregation was fully suppressed by 100 μM macrocycle **1a** and was delayed by 25 and 50 μM macrocycle **1a**. This result indicates that macrocycle **1a** can also suppress AcPHF6 aggregation for the duration of the assay at substoichiometric concentrations.

(33) Pauling, L.; Corey, R. B. *Proc. Natl. Acad. Sci. U.S.A.* **1951**, *37*, 251–256.

(34) Chung, D. M.; Nowick, J. S. *J. Am. Chem. Soc.* **2004**, *126*, 3062–3063.

(35) A detailed description of the X-ray crystallographic structure and intermolecular packing mode of macrocycle **1h** and several related macrocycles will be elaborated in a separate paper.

(36) Khakshoor, O.; Demeler, B.; Nowick, J. S. *J. Am. Chem. Soc.* **2007**, *129*, 5558–5569.

(37) Khakshoor, O.; Nowick, J. S. *Org. Lett.* **2009**, *11*, 3000–3003.

(38) Wishart, D. S.; Sykes, B. D. *Methods Enzymol.* **1994**, *239*, 363–392.

(39) A "dock−lock" mechanism has been proposed for the growth of the more complex β-amyloid ($A\beta_{1-40}$) by Maggio and co-workers: Esler, W. P.; Stimson, E. R.; Jennings, J. M.; Vinters, H. V.; Ghilardi, J. R.; Lee, J. P.; Mantyh, P. W.; Maggio, J. E. *Biochemistry* **2000**, *39*, 6288–6295.

(40) Sciarretta, K. L.; Gordon, D. J.; Meredith, S. C. *Methods Enzymol.* **2006**, *413*, 273–312.

(41) (a) Gordon, D. J.; Sciarretta, K. L.; Meredith, S. C. *Biochemistry* **2001**, *40*, 8237–8245. (b) Kokkoni, N.; Stott, K.; Amijee, H.; Mason, J. M.; Doig, A. J. *Biochemistry* **2006**, *45*, 9906–9918. (c) Madine, J.; Doig, A. J.; Middleton, D. A. *J. Am. Chem. Soc.* **2008**, *130*, 7873–7881.

(42) (a) Etienne, M. A.; Aucoin, J. P.; Fu, Y. W.; McCarley, R. L.; Hammer, R. P. *J. Am. Chem. Soc.* **2006**, *128*, 3522–3523. (b) Bett, C. K.; Ngunjiri, J. N.; Serem, W. K.; Fontenot, K. R.; Hammer, R. P.; McCarley, R. L.; Garno, J. C. *ACS Chem. Neurosci.* **2010**, *1*, 608–626.

(43) Gordon, D. J.; Meredith, S. C. *Biochemistry* **2003**, *42*, 475–485.

(44) Soto, C.; Sigurdsson, E. M.; Morelli, L.; Kumar, R. A.; Castano, E. M.; Frangione, B. *Nat. Med.* **1998**, *4*, 822–826.

(45) Glabe, C. G. *Neurobiol. Aging* **2006**, *27*, 570–575.

(46) Haass, C.; Selkoe, D. J. *Nat. Rev. Mol. Cell Biol.* **2007**, *8*, 101–112.

(47) Ono, K.; Condron, M. M.; Teplow, D. B. *Proc. Natl. Acad. Sci. U.S.A.* **2009**, *106*, 14745–14750.

(48) Mc Donald, J. M.; Savva, G. M.; Brayne, C.; Welzel, A. T.; Forster, G.; Shankar, G. M.; Selkoe, D. J.; Ince, P. G.; Walsh, D. M.; Function, M. R. C. C. *Brain* **2010**, *133*, 1328–1341.

(49) Shankar, G. M.; Li, S. M.; Mehta, T. H.; Garcia-Munoz, A.; Shepardson, N. E.; Smith, I.; Brett, F. M.; Farrell, M. A.; Rowan, M. J.; Lemere, C. A.; Regan, C. M.; Walsh, D. M.; Sabatini, B. L.; Selkoe, D. J. *Nat. Med.* **2008**, *14*, 837–842.

(50) Yu, L. P.; et al. *Biochemistry* **2009**, *48*, 1870–1877.

(51) Moore, B. D.; Rangachari, V.; Tay, W. M.; Milkovic, N. M.; Rosenberry, T. L. *Biochemistry* **2009**, *48*, 11796–11806.

(52) Ahmed, M.; Davis, J.; Aucoin, D.; Sato, T.; Ahuja, S.; Aimoto, S.; Elliott, J. I.; Van Nostrand, W. E.; Smith, S. O. *Nat. Struct. Mol. Biol.* **2010**, *17*, 561–567.

(53) (a) Opar, A. *Nat. Rev. Drug Discovery* **2008**, *7*, 717–718. (b) Extance, A. *Nat. Rev. Drug Discovery* **2010**, *9*, 749–751.

(54) Bulic, B.; Pickhardt, M.; Schmidt, B.; Mandelkow, E. M.; Waldmann, H.; Mandelkow, E. *Angew. Chem., Int. Ed.* **2009**, *48*, 1740–1752.

(55) Brunden, K. R.; Trojanowski, J. Q.; Lee, V. M. *Nat. Rev. Drug Discovery* **2009**, *8*, 783–793.

(56) Biron, E.; Chatterjee, J.; Kessler, H. *J. Pept. Sci.* **2006**, *12*, 213–219.

(57) In initially developing the ThS fluorescence assay conditions, we quantified AcPHF6 and macrocycle **1a** solutions both gravimetrically and spectrophotometrically. The gravimetrically and spectrophotometrically determined concentrations of the peptide were found to match within ±10%. In subsequent studies, we prepared all solutions gravimetrically and consider concentrations accurate to ±10%.

(58) Initially we tried using Teflon mixing balls in the wells, but we found that the data were more reproducible and less noisy without mixing balls. Teflon mixing balls are commonly used in ThT fluorescence assays of Aβ aggregation.